International Journal of
Network Dynamics and Intelligence (IJNDI)

Scilight

Article

Finite-Horizon H_∞ Control for Mobile Robots under Hybrid Cyber Attacks: An Accumulation-Based Event-Triggered Mechanism

Baoye Song *, Bingna Sun, and Jiqing Zhang

The College of Electrical Engineering and Automation, Shandong University of Science and Technology, Qingdao 266590, China
* Correspondence: songbaoye@sdust.edu.cn
Received: 28 September 2025; Revised: 23 November 2025; Accepted: 15 January 2026; Published: 9 March 2026

Abstract: This paper investigates the finite-horizon H_∞ control problem for mobile robot system under hybrid cyber attacks, where signal transmissions from sensors to the controller are scheduled using an accumulation-based event-triggered mechanism (AETM) to reduce communication load. Compared with traditional event-triggered strategies, the AETM exhibits enhanced robustness against burst signals and owns a lower communication frequency. A more general cyber attack scenario is considered, in which randomly occurring denial-of-service (DoS) attacks and deception attacks coexist, forming a hybrid attack environment. The objective is to develop an AETM-based control strategy that ensures the mobile robot system satisfies the desired finite-horizon H_∞ performance under such hybrid attacks. Sufficient conditions are first derived using the stochastic analysis technique to guarantee that the mobile robot system meets the prescribed control performance under the proposed strategy. Then, by recursively solving a sequence of matrix inequalities, a time-varying controller gain is computed in real time. Finally, the effectiveness of the proposed controller is demonstrated through numerical simulations based on the kinematic model of a mobile robot.

Keywords: mobile robot; accumulation-based event-triggered mechanism; finite-horizon H_∞ control; hybrid attack; matrix inequality

1. Introduction

With the rapid advancement of 5G communication and Internet of Things (IoT) technologies, mobile robot systems have achieved more efficient resource scheduling and task allocation through cloud-based data sharing and distributed computation. These advancements have significantly enhanced the cooperative capabilities and remote control accuracy of mobile robots, enabling their widespread application in areas such as intelligent logistics, smart urban transportation, and domestic services [1]. Currently, the networked control of mobile robots has become a prominent research topic. A main challenge to the control of mobile robots is the so-called network-induced phenomena resulted from inherently limited bandwidth such as communication delays, packet loss, and congestion. If not properly addressed, these phenomena may severely compromise the stability of the mobile robot system [2–5].

To address the limitations imposed by constrained network bandwidth, event-triggered mechanisms (ETMs), which dynamically regulate the frequency of data transmissions based on predefined triggering conditions, have been extensively employed [6–9]. Specifically, information with ETMs is transmitted only when predetermined triggering conditions are met, thereby significantly reducing communication load compared to traditional time-triggered schemes [10]. To further enhance communication efficiency, various improved ETMs have been developed based on the traditional ETM framework [11]. For instance, a dynamic ETM has been proposed in [12], where an auxiliary dynamic variable has been introduced to construct a new triggering condition. In [13], an adaptive memory-based ETM has been proposed to address the control problem of TCS fuzzy systems under asynchronous premise variables. In [14], an accumulation-based event-triggered mechanism (AETM) has been developed to investigate the joint state and actuator fault estimation problem. Among these improved ETMs, the AETM achieves a lower transmission frequency and enhanced robustness against burst signals compared to traditional ETMs. Despite these advantages, the application of the AETM to the finite-horizon H_∞ control problem for mobile robots remains unexplored, which serves as one of the motivations for this paper.

Moreover, the openness of network channels makes the transmitted information vulnerable to malicious cyber attacks, which may lead to system malfunctions or even complete failures [15]. Extensive research has been conducted on various types of cyber attacks [16], which are generally classified into three categories: denial-of-service (DoS) attacks [17, 18], and deception attacks [19–22]. Among them, DoS attacks inject large volumes

of irrelevant data into shared communication channels, leading to network congestion and potentially paralyzing the system [23]. Deception attacks aim to mislead system decisions or alter operational states by injecting false information to override or replace valid data [24]. As cyber attack and defense strategies continue to evolve, single-type attacks have become insufficient to meet attackers objectives. Consequently, hybrid cyber attacks, in which multiple types of attacks coexist, have emerged as one of the most challenging issues in contemporary network security [25]. In the context of finite-horizon H_∞ control for mobile robots under AETMs, addressing the secure control problem posed by hybrid cyber attacks constitutes another major motivation of this paper.

Based on the above discussions, the finite-horizon H_∞ control problem for mobile robots under AETMs and hybrid cyber attacks is both theoretically and practically significant problems. Nevertheless, this problem is far from straightforward due to several major challenges: (1) how to derive sufficient conditions under which the mobile robot system satisfies the desired finite-horizon H_∞ performance in the presence of coupled AETM scheduling and hybrid cyber attacks? and (2) how to determine the corresponding controller gains to guarantee the desired control performance? This paper aims to address these two questions. The main contributions are summarized as follows:

(1) The finite-horizon H_∞ control problem is investigated, for the first time, for mobile robots under hybrid cyber attacks and AETMs.
(2) Sufficient conditions are established to ensure that the mobile robot system satisfies the finite-horizon H_∞ performance under the coupling of hybrid cyber attacks and AETMs.
(3) By recursively solving a set of matrix inequalities, the time-varying controller gains are computed online, thereby facilitating the practical implementation of the control algorithm.

The remainder of this paper is organized as follows. Section 2 formulates the finite-horizon H_∞ control problem for mobile robots under AETM scheduling and randomly occurring hybrid cyber attacks. In Section 3, sufficient conditions are established to ensure that the system satisfies the finite-horizon H_∞ performance, and the corresponding controller design is presented. Section 4 provides numerical simulations based on a kinematic model of a mobile robot to demonstrate the effectiveness of the designed controller. Finally, Section 5 concludes this paper.

2. Problem Formulation and Preliminaries

The structure diagram of the system is shown in Figure 1. During the data transmission from the sensor to the controller, the signals are first scheduled by the AETM, and only those satisfying the triggering condition are allowed to be transmitted. During the transmission process, the data may be affected by randomly occurring hybrid cyber attacks. In the following, we sequentially present the system model, the AETM, the hybrid cyber attack model, and the adopted controller structure.

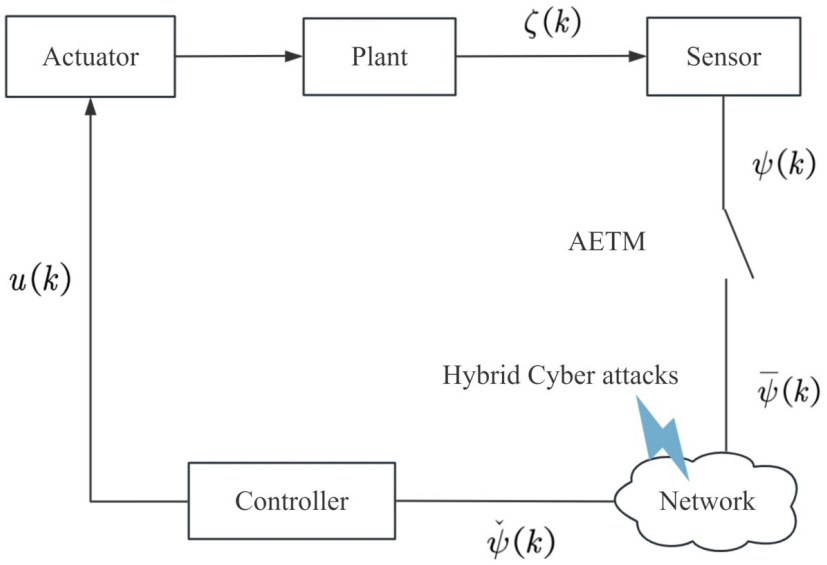

Figure 1. The structure diagram of the system.

2.1. System Model

In this paper, a kinematics-based model of a wheeled mobile robot is considered. As illustrated in Figure 2, a global coordinate frame XOY fixed in the workspace and a body-fixed coordinate frame xoy attached to the robot's center of mass are established. The kinematic model of the mobile robot is described as follows:

$$\begin{cases} \dot{x}(k) = v(k)\cos\theta(k) \\ \dot{y}(k) = v(k)\sin\theta(k) \\ \dot{\theta}(k) = \dfrac{v(k)\tan\varphi(k)}{l} \end{cases} \tag{1}$$

where the position of the robot's center of mass is denoted by $(x(k), y(k))$; l represents the distance between the front and rear wheels; the variables $v(k)$ and $\varphi(k)$ denote the linear velocity and the front wheel steering angle, respectively; and $\theta(k)$ represents the robot's heading angle.

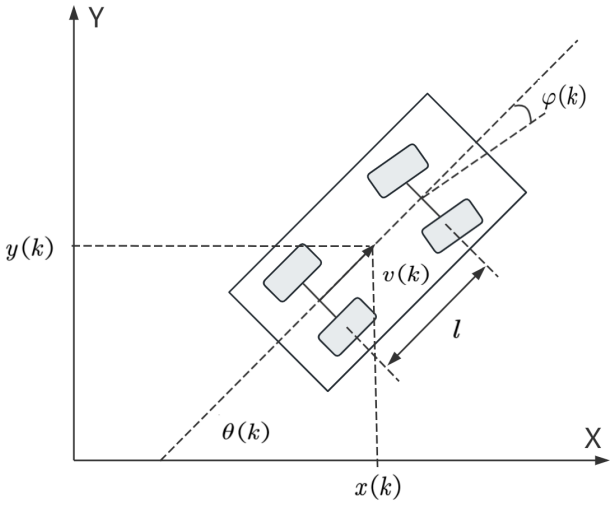

Figure 2. Model of the mobile robot.

Define

$$\chi(k) \triangleq \begin{bmatrix} x(k) & y(k) & \theta(k) \end{bmatrix}^T$$

and

$$\varpi(k) \triangleq \begin{bmatrix} v(k) & \varphi(k) \end{bmatrix}^T.$$

Given the reference trajectory point $\chi_r(k) \triangleq \begin{bmatrix} x_r(k) & y_r(k) & \theta_r(k) \end{bmatrix}^T$ and the corresponding input $\varpi_r(k) \triangleq \begin{bmatrix} v_r(k) & \varphi_r(k) \end{bmatrix}^T$, the kinematic model of the mobile robot can be linearized around the reference trajectory point as follows:

$$\begin{aligned} \dot{\chi}(k) - \dot{\chi_r}(k) \simeq & \begin{bmatrix} 0 & 0 & -v_r(k)\sin\theta_r(k) \\ 0 & 0 & v_r(k)\cos\theta_r(k) \\ 0 & 0 & 0 \end{bmatrix} (\chi(k) - \chi_r(k)) \\ & + \begin{bmatrix} \cos\theta_r(k) & 0 \\ \sin\theta_r(k) & 0 \\ \frac{\tan\theta_r(k)}{l} & \frac{v_r(k)}{l\cos^2\varphi_r(k)} \end{bmatrix} (\varpi(k) - \varpi_r(k)). \end{aligned} \tag{2}$$

By introducing the tracking error state $\zeta(k) \triangleq \chi(k) - \chi_r(k)$ and the control deviation $u(k) \triangleq \varpi(k) - \varpi_r(k)$, the trajectory tracking problem of the mobile robot is transformed into a stabilization problem of the tracking error system. The resulting model is then discretized as follow:

$$\begin{aligned} \zeta(k+1) \simeq & \begin{bmatrix} 1 & 0 & -Tv_r(k)\sin\theta_r(k) \\ 0 & 1 & Tv_r(k)\cos\theta_r(k) \\ 0 & 0 & 1 \end{bmatrix} \zeta(k) \\ & + \begin{bmatrix} T\cos\theta_r(k) & 0 \\ T\sin\theta_r(k) & 0 \\ T\frac{\tan\theta_r(k)}{l} & T\frac{v_r(k)}{l\cos^2\varphi_r(k)} \end{bmatrix} u(k) \end{aligned} \tag{3}$$

where T is the sampling period. To account for the influence of noise in practical environments, the model is further extended as follows:

$$\begin{cases} \zeta(k+1) = A(k)\zeta(k) + B(k)u(k) + E(k)\omega(k) \\ \psi(k) = C(k)\zeta(k) + D(k)\nu(k) \\ z(k) = M(k)\zeta(k) \end{cases} \tag{4}$$

where $\psi(k) \in \mathbb{R}^{n_\psi}$ is the measurement output; $z(k) \in \mathbb{R}^{n_z}$ denotes the desired state to be controlled; the matrices $C(k)$, $D(k)$, $E(k)$, and $M(k)$ are time-varying with appropriate dimensions; $\nu(k) \in l_2([0, \mathcal{T}-1]; \mathbb{R}^{n_\nu})$ and $\omega(k) \in l_2([0, \mathcal{T}-1]; \mathbb{R}^{n_\omega})$ are energy-bounded measurement noise and process noise, respectively; and $\mathcal{T}$ denotes the given finite horizon.

2.2. Event Generator

In this section, an AETM is employed to reduce the frequency of data transmissions between the sensor and the controller over the network, thereby conserving communication resources. Under this mechanism, the measured output is transmitted to the remote controller only when a prescribed event-triggering condition is satisfied. The AETM is described in detail as follows.

Let the sequence of the triggering instants be $0 = k_0 < k_1 < k_2 < \cdots < k_s < \cdots$, and define the event generator function $\rho : \mathbb{R} \times \mathbb{R} \times \mathbb{R}^{n_\psi} \to \mathbb{R}$ as

$$\rho(\alpha, \theta, \xi(k)) = \sum_{\tilde{i}=k_s}^{k} \left(\alpha^{k-\tilde{i}} \left(\theta - \xi^T(\tilde{i}) \xi(\tilde{i}) \right) \right) \tag{5}$$

where $\xi(\tilde{i}) \triangleq \psi(\tilde{i}) - \psi(k_s)$; $\alpha \in (0,1)$ is a given weighting coefficient; $\theta > 0$ is a prescribed tunable parameter; and k_s denotes the most recent triggering instant prior to time k. The next triggering instant is determined according to

$$k_{s+1} \triangleq \min\{k \mid k > k_s,\ \rho(\alpha, \theta, \xi(k)) \leq 0\}. \tag{6}$$

Remark 1. *As shown in (5), the AETM determines the triggering instants based on the accumulated error over a time interval. Compared with conventional triggering mechanisms that rely solely on the instantaneous error, this scheme effectively mitigates the adverse impact of abrupt signal variations and enhances robustness against undesirable signal fluctuations.*

2.3. Hybrid Cyber Attacks

Due to the openness of wireless communication, the data transmission process is susceptible to cyber attacks. In this paper, it is considered that the communication between the sensor and the controller is subject to randomly occurring DoS attacks and deception attacks. The signal received by the controller, denoted as $\bar{\psi}(k_s)$, can be expressed as follows:

$$\bar{\psi}(k_s) = \psi(k_s) + \alpha(k)\beta(k)\mu(k) + \alpha(k)(1 - \beta(k))\varpi(k) \tag{7}$$

where $\mu(k)$ and $\varpi(k)$ are the deception attack and the DoS attack launched by the attackers, respectively. They can be described as follows:

$$\mu(k) = -\psi(k_s) + \varsigma(k) \tag{8}$$

and

$$\varpi(k) = -\psi(k_s) \tag{9}$$

where $\varsigma \in l_2([0, \mathcal{T}-1]; \mathbb{R}^{n_\varsigma})$. $\alpha(k)$ and $\beta(k)$ satisfy the following statistical properties:

$$\begin{aligned} &\text{prob}\{\alpha(k) = 1\} = \bar{\alpha}, \quad \text{prob}\{\alpha(k) = 0\} = 1 - \bar{\alpha}, \\ &\text{prob}\{\beta(k) = 1\} = \bar{\beta}, \quad \text{prob}\{\beta(k) = 0\} = 1 - \bar{\beta} \end{aligned} \tag{10}$$

where $\bar{\alpha} \in$ [1,0) and $\bar{\beta} \in$ [1,0) are known constants.

By employing the zero-order holder mechanism, the input signal of the controller can be expressed as

$$\begin{aligned}\check{\psi}(k) \triangleq &(1-\alpha(k))\psi(k_s)\\ &+\alpha(k)\beta(k)\varsigma(k), \forall k \in [k_s, k_{s+1}), s \geq 0.\end{aligned} \tag{11}$$

Remark 2. *Based on the above expression, it is easy to observe that when $\alpha(k) = 0$, the controller receives the normal signal. When $\alpha(k) = 1$ and $\beta(k) = 0$, the data transmission is subject to the DoS attack. When $\alpha(k) = 1$ and $\beta(k) = 1$, the data transmission is subject to the deception attack.*

2.4. Structure of the Controller

According to the previous discussion, the following controller is contructed:

$$u(k) = K(k)\check{\psi}(k) \tag{12}$$

where $K(k)$ $(0 \leq k \leq \mathcal{T}-1)$ denotes the time-varying controller gain to be determined. By substituting (12) into (4), the closed-loop system dynamics can be obtained as:

$$\zeta(k+1) = A(k)\zeta(k) + B(k)K(k)\check{\psi}(k) + E(k)\omega(k). \tag{13}$$

Based on (4), (5), (7), and (12), we have

$$\begin{aligned}\zeta(k+1) =&A(k)\zeta(k) + (1-\alpha(k))B(k)K(k)\psi(k_s)\\ &+\alpha(k)\beta(k)B(k)K(k)\varsigma(k) + E(k)\omega(k)\\ =&A(k)\zeta(k) + (1-\alpha(k))B(k)K(k)(\psi(k)-\xi(k))\\ &+\alpha(k)\beta(k)B(k)K(k)\varsigma(k) + E(k)\omega(k)\\ =&\big(A(k) + (1-\alpha(k))B(k)K(k)C(k)\big)\zeta(k)\\ &+(1-\alpha(k))B(k)K(k)D(k)\nu(k)\\ &-(1-\alpha(k))B(k)K(k)\xi(k)\\ &+\alpha(k)\beta(k)B(k)K(k)\varsigma(k) + E(k)\omega(k)\\ =&\big(A(k) + (1-\bar{\alpha})B(k)K(k)C(k)\\ &+(\bar{\alpha}-\alpha(k))B(k)K(k)C(k)\big)\zeta(k)\\ &+\big((1-\bar{\alpha})B(k)K(k)D(k)\\ &+(\bar{\alpha}-\alpha(k))B(k)K(k)D(k)\big)\nu(k)\\ &-\big((1-\bar{\alpha})B(k)K(k)\\ &+(\bar{\alpha}-\alpha(k))B(k)K(k)\big)\xi(k)\\ &+(\alpha(k)\beta(k)-\bar{\alpha}\bar{\beta})B(k)K(k)\varsigma(k)\\ &+\bar{\alpha}\bar{\beta}B(k)K(k)\varsigma(k) + E(k)\omega(k)\\ =&\big(\mathcal{A}_1(k) + \tilde{\alpha}(k)\mathcal{A}_2(k)\big)\zeta(k)\\ &+\big(\mathcal{A}_3(k) + \tilde{\alpha}(k)\mathcal{A}_4(k)\big)\nu(k) - \big(\mathcal{A}_5(k)\\ &+\tilde{\alpha}(k)\mathcal{A}_6(k)\big)\xi(k) + \big(\mathcal{A}_7(k) + \tilde{\tau}(k)\mathcal{A}_6(k)\big)\varsigma(k)\\ &+E(k)\omega(k)\end{aligned} \tag{14}$$

where

$$\begin{aligned}&\tilde{\alpha}(k) \triangleq \bar{\alpha} - \alpha(k), \tilde{\beta}(k) \triangleq \bar{\beta} - \beta(k), \tilde{\tau}(k) \triangleq \alpha(k)\beta(k) - \bar{\alpha}\bar{\beta},\\ &\mathcal{A}_1(k) \triangleq A(k) + (1-\bar{\alpha})B(k)K(k)C(k),\\ &\mathcal{A}_2(k) \triangleq B(k)K(k)C(k),\\ &\mathcal{A}_3(k) \triangleq (1-\bar{\alpha})B(k)K(k)D(k), \mathcal{A}_4(k) \triangleq B(k)K(k)D(k),\\ &\mathcal{A}_5(k) \triangleq (1-\bar{\alpha})B(k)K(k), \mathcal{A}_6(k) \triangleq B(k)K(k),\\ &\mathcal{A}_7(k) \triangleq \bar{\alpha}\bar{\beta}B(k)K(k).\end{aligned}$$

Define $\bar{\omega}(k) \triangleq \begin{bmatrix}\omega^T(k) & \nu^T(k) & \varsigma^T(k)\end{bmatrix}^T$. It follows from (14) that

$$\begin{cases}\zeta(k+1) = \big(\mathcal{A}_1(k) + \tilde{\alpha}(k)\mathcal{A}_2(k)\big)\zeta(k) \\ \qquad\qquad + \big(\mathcal{L}_1(k) + \tilde{\alpha}(k)\mathcal{L}_2(k) + \tilde{\tau}(k)\mathcal{L}_3(k)\big)\bar{\omega}(k) \\ \qquad\qquad - \big(\mathcal{A}_5(k) + \tilde{\alpha}(k)\mathcal{A}_6(k)\big)\xi(k) \\ z(k) = M(k)\zeta(k)\end{cases} \tag{15}$$

where

$$\mathcal{L}_1(k) \triangleq \begin{bmatrix}E(k) & \mathcal{A}_3(k) & \mathcal{A}_7(k)\end{bmatrix},$$
$$\mathcal{L}_2(k) \triangleq \begin{bmatrix}0 & \mathcal{A}_4(k) & 0\end{bmatrix}, \mathcal{L}_3(k) \triangleq \begin{bmatrix}0 & 0 & \mathcal{A}_6(k)\end{bmatrix}.$$

The main objective of this paper is to ensure that, over the given finite horizon $[0, \mathcal{T}-1]$, the system state in (15) satisfies the following finite-horizon H_∞ performance

$$\begin{aligned}&\mathbb{E}\left\{\sum_{k=0}^{\mathcal{T}-1}(z^T(k)z(k))\right\} \\ &\leq \mathbb{E}\left\{\gamma^2\Big(\sum_{k=0}^{\mathcal{T}-1}\big(\bar{\omega}^T(k)\bar{\omega}(k) + \varrho + \zeta^T(0)W\zeta(0)\big)\Big)\right\}\end{aligned} \tag{16}$$

where W is a given positive definite matrix and ϱ is a given positive scalar.

3. Main Results

This section first provides a sufficient condition for guaranteeing that the designed controller satisfies the performance in (16). Subsequently, the controller gain is obtained by recursively solving a set of matrix inequalities.

Theorem 1. *Let the controller gains $K(k)$ $(0 \leq k \leq \mathcal{T}-1)$, positive scalars $\gamma > 0$, $0 < \alpha < 1$, $\theta > 0$, $\varrho > 0$, and a positive definite matrix W be given. Assume that there exist matrices $P(k)$ and $\Gamma(k)$, and a scalar a_1 such that, under the initial conditions $P(0) \leq \gamma^2 W$, the following matrix inequalities are satisfied:*

$$\Lambda(k) = \begin{bmatrix}\Lambda_{11}(k) & \Lambda_{12}(k) & \Lambda_{13}(k) \\ * & \Lambda_{22}(k) & \Lambda_{23}(k) \\ * & * & \Lambda_{33}(k)\end{bmatrix} < 0 \tag{17}$$

$$\Gamma(k) < \gamma^2 I \tag{18}$$

$$a_1\frac{\theta}{1-\alpha} \leq \gamma^2\varrho \tag{19}$$

for each $k \in [0, \mathcal{T}-2]$, where

$$\begin{aligned}\check{\alpha} \triangleq& \bar{\alpha} - \bar{\alpha}^2, \check{\beta} \triangleq \bar{\beta} - \bar{\beta}^2, \check{\tau} \triangleq \bar{\alpha}\bar{\beta} - \bar{\alpha}^2\bar{\beta}^2, o \triangleq \sqrt{\check{\alpha}\check{\tau}}, \\ \Lambda_{11}(k) \triangleq& \mathcal{A}_1^T(k)P(k+1)\mathcal{A}_1(k) + \check{\alpha}\mathcal{A}_2^T(k)P(k+1)\mathcal{A}_2(k) \\ &- P(k) + M^T(k)M(k), \\ \Lambda_{12}(k) \triangleq& \mathcal{A}_1^T(k)P(k+1)\mathcal{L}_1(k) + \check{\alpha}\mathcal{A}_2^T(k)P(k+1)\mathcal{L}_2(k) \\ &+ o\mathcal{A}_2^T(k)P(k+1)\mathcal{L}_3(k), \\ \Lambda_{13}(k) \triangleq& -\mathcal{A}_1^T(k)P(k+1)\mathcal{A}_5(k) \\ &- \check{\alpha}\mathcal{A}_2^T(k)P(k+1)\mathcal{A}_6(k), \\ \Lambda_{22}(k) \triangleq& \mathcal{L}_1^T(k)P(k+1)\mathcal{L}_1(k) + \check{\alpha}\mathcal{L}_2^T(k)P(k+1)\mathcal{L}_2(k) \\ &+ 2o\mathcal{L}_2^T(k)P(k+1)\mathcal{L}_3(k) - \Gamma(k) \\ &+ \check{\tau}(k)\mathcal{L}_3^T(k)P(k+1)\mathcal{L}_3(k),\end{aligned}$$

$$\begin{aligned}\Lambda_{23}(k) \triangleq & -\mathcal{L}_1^T(k)P(k+1)\mathcal{A}_5(k) - \check{\alpha}\mathcal{L}_2^T(k)P(k+1)\\ & \times \mathcal{A}_6(k) - o\mathcal{L}_3^T(k)P(k+1)\mathcal{A}_6(k),\\ \Lambda_{33}(k) \triangleq & \mathcal{A}_5^T(k)P(k+1)\mathcal{A}_5(k)\\ & + \check{\alpha}\mathcal{A}_6^T(k)P(k+1)\mathcal{A}_6(k) - a_1.\end{aligned}$$

Then, the system (15) achieves the finite-horizon H_∞ performance (16).

Proof. The Lyapunov-like functional is constructed as follows:

$$V(k) = \zeta^T(k)P(k)\zeta(k) \tag{20}$$

Denoting

$$\Delta\mathcal{V}(k) \triangleq \mathcal{V}(k+1) - \mathcal{V}(k),$$

we can obtain that

$$\begin{aligned}&\mathbb{E}\{\Delta V(k)\} = \mathbb{E}\big\{V(k+1) - V(k)\big\}\\ =&\mathbb{E}\Big\{\zeta^T(k+1)P(k+1)\zeta(k+1) - \zeta^T(k)P(k)\zeta(k)\Big\}\\ =&\mathbb{E}\Bigg\{\Bigg(\big(\mathcal{A}_1(k) + \tilde{\alpha}(k)\mathcal{A}_2(k)\big)\zeta(k) + \big(\mathcal{L}_1(k) + \tilde{\alpha}(k)\mathcal{L}_2(k)\\ &+ \tilde{\tau}(k)\mathcal{L}_3(k)\big)\bar{\omega}(k) - \big(\mathcal{A}_5(k) + \tilde{\alpha}(k)\mathcal{A}_6(k)\big)\xi(k)\Bigg)^T\\ &\times P(k+1)\Bigg(\big(\mathcal{A}_1(k) + \tilde{\alpha}(k)\mathcal{A}_2(k)\big)\zeta(k) + \big(\mathcal{L}_1(k)\\ &+ \tilde{\alpha}(k)\mathcal{L}_2(k) + \tilde{\tau}(k)\mathcal{L}_3(k)\big)\bar{\omega}(k) - \big(\mathcal{A}_5(k)\\ &+ \tilde{\alpha}(k)\mathcal{A}_6(k)\big)\xi(k)\Bigg) - \zeta^T(k)P(k)\zeta(k)\Bigg\}.\end{aligned} \tag{21}$$

According to (10), we have

$$\begin{aligned}\mathbb{E}\{\tilde{\alpha}(k)\} &= \mathbb{E}\{\bar{\alpha}\} - \mathbb{E}\{\alpha(k)\}\\ &= \bar{\alpha} - (1\times\bar{\alpha} + 0\times(1-\bar{\alpha}))\\ &= 0,\end{aligned}$$

and

$$\begin{aligned}\mathbb{E}\{\tilde{\alpha}(k)^2\} &= \mathbb{E}\{(\mathbb{E}\{\alpha(k)\} - \alpha(k))^2\}\\ &= \mathbb{E}\{(\mathbb{E}\{\alpha(k)\})^2 - 2\mathbb{E}\{\alpha(k)\}\alpha(k) + \alpha^2(k)\}\\ &= \mathbb{E}^2\{\alpha(k)\} - 2(\mathbb{E}\{\alpha(k)\})^2 + \mathbb{E}\{\alpha^2(k)\}\\ &= \mathbb{E}\{\alpha^2(k)\} - (\mathbb{E}\{\alpha(k)\})^2\\ &= 1^2\times\bar{\alpha} + 0^2\times(1-\bar{\alpha}) - \bar{\alpha}^2\\ &= \bar{\alpha} - \bar{\alpha}^2.\end{aligned}$$

Similarly, we can conclude that $\mathbb{E}\{\tilde{\beta}(k)\} = 0, \mathbb{E}\{\tilde{\beta}^2(k)\} = \bar{\beta} - \bar{\beta}^2, \mathbb{E}\{\tilde{\tau}(k)\} = 0, \mathbb{E}\{\tilde{\tau}^2(k)\} = \bar{\alpha}\bar{\beta} - \bar{\alpha}^2\bar{\beta}^2$. Denoting $\check{\alpha} \triangleq \bar{\alpha} - \bar{\alpha}^2$, $\check{\beta} \triangleq \bar{\beta} - \bar{\beta}^2$, and $\check{\tau} \triangleq \bar{\alpha}\bar{\beta} - \bar{\alpha}^2\bar{\beta}^2$, we can obtain that

$$\begin{aligned}\mathbb{E}\{\tilde{\alpha}(k)\tilde{\tau}(k)\} &= \bar{\alpha}\bar{\beta} - \bar{\alpha}^2\bar{\beta}\\ &\leq \mathbb{E}\{\sqrt{\check{\alpha}\check{\tau}}\}\\ &= \sqrt{\bar{\alpha}^2\bar{\beta} - \bar{\alpha}^3\bar{\beta}^2 - \alpha^3\bar{\beta} + \bar{\alpha}^4\bar{\beta}^2}.\end{aligned}$$

Then, (21) can be rewritten as

$$\begin{aligned}
&\mathbb{E}\{\Delta V(k)\}\\
=&\mathbb{E}\Big\{\zeta^T(k)\Big(\mathcal{A}_1^T(k)P(k+1)\mathcal{A}_1(k)+\check{\alpha}\mathcal{A}_2^T(k)P(k+1)\\
&\times\mathcal{A}_2(k)-P(k)\Big)\zeta(k)+\bar{\omega}^T(k)\big(\mathcal{L}_1^T(k)P(k+1)\mathcal{L}_1(k)\\
&+\check{\alpha}\mathcal{L}_2^T(k)P(k+1)\mathcal{L}_2(k)+2\tilde{\alpha}(k)\tilde{\tau}(k)\mathcal{L}_2^T(k)P(k+1)\\
&\times\mathcal{L}_3(k)+\check{\tau}(k)\mathcal{L}_3^T(k)P(k+1)\mathcal{L}_3(k)\Big)\bar{\omega}(k)+\xi^T(k)\\
&\times\Big(\mathcal{A}_5^T(k)P(k+1)\mathcal{A}_5(k)+\check{\alpha}\mathcal{A}_6^T(k)P(k+1)\mathcal{A}_6(k)\Big)\\
&\times\xi(k)+2\zeta^T(k)\Big(\mathcal{A}_1^T(k)P(k+1)\mathcal{L}_1(k)+\check{\alpha}\mathcal{A}_2^T(k)\Big)\\
&\times P(k+1)\mathcal{L}_2\Big(k+\tilde{\alpha}(k)\tilde{\tau}(k)\mathcal{A}_2^T(k)P(k+1)\mathcal{L}_3(k)\Big)\bar{\omega}(k)\\
&+2\zeta^T(k)\Big(-\mathcal{A}_1^T(k)P(k+1)\mathcal{A}_5(k)-\check{\alpha}\mathcal{A}_2^T(k)P(k+1)\\
&\times\mathcal{A}_6(k)\Big)\xi(k)+2\bar{\omega}^T(k)\Big(-\mathcal{L}_1^T(k)P(k+1)\mathcal{A}_5(k)\\
&-\check{\alpha}\mathcal{L}_2^T(k)P(k+1)\mathcal{A}_6(k)-\tilde{\alpha}(k)\tilde{\tau}(k)\mathcal{L}_3^T(k)\\
&\times P(k+1)\mathcal{A}_6(k)\Big)\xi(k)\Big\}\\
<&\mathbb{E}\{\mathcal{J}^T(k)\mathscr{H}(k)\mathcal{J}(k)\}
\end{aligned}\tag{22}$$

where

$$\begin{aligned}
\mathscr{H}(k)\triangleq&\begin{bmatrix}\mathscr{H}_{11}(k)&\mathscr{H}_{12}(k)&\mathscr{H}_{13}(k)\\ *&\mathscr{H}_{22}(k)&\mathscr{H}_{23}(k)\\ *&*&\mathscr{H}_{33}(k)\end{bmatrix},\\
\mathcal{J}(k)\triangleq&\begin{bmatrix}\zeta^T(k)&\bar{\omega}^T(k)&\xi^T(k)\end{bmatrix}^T,\\
\mathscr{H}_{11}(k)\triangleq&\mathcal{A}_1^T(k)P(k+1)\mathcal{A}_1(k)+\check{\alpha}\mathcal{A}_2^T(k)P(k+1)\mathcal{A}_2(k)\\
&-P(k),\\
\mathscr{H}_{12}(k)\triangleq&\mathcal{A}_1^T(k)P(k+1)\mathcal{L}_1(k)+\check{\alpha}\mathcal{A}_2^T(k)P(k+1)\mathcal{L}_2(k)\\
&+o\mathcal{A}_2^T(k)P(k+1)\mathcal{L}_3(k),\\
\mathscr{H}_{13}(k)\triangleq&-\mathcal{A}_1^T(k)P(k+1)\mathcal{A}_5(k)-\check{\alpha}\mathcal{A}_2^T(k)P(k+1)\\
&\times\mathcal{A}_6(k),\\
\mathscr{H}_{22}(k)\triangleq&\mathcal{L}_1^T(k)P(k+1)\mathcal{L}_1(k)+\check{\alpha}\mathcal{L}_2^T(k)P(k+1)\mathcal{L}_2(k)\\
&+2o\mathcal{L}_2^T(k)P(k+1)\mathcal{L}_3(k)+\check{\tau}(k)\mathcal{L}_3^T(k)\\
&\times P(k+1)\mathcal{L}_3(k),\\
\mathscr{H}_{23}(k)\triangleq&-\mathcal{L}_1^T(k)P(k+1)\mathcal{A}_5(k)-\check{\alpha}\mathcal{L}_2^T(k)P(k+1)\\
&\times\mathcal{A}_6(k)-o\mathcal{L}_3^T(k)P(k+1)\mathcal{A}_6(k),\\
\mathscr{H}_{33}(k)\triangleq&\mathcal{A}_5^T(k)P(k+1)\mathcal{A}_5(k)+\check{\alpha}\mathcal{A}_6^T(k)P(k+1)\mathcal{A}_6(k).
\end{aligned}$$

Based on (5) and (6), we arrive at

$$\sum_{t=k_r}^{k_{r+1}-1}(\alpha^{k_{r+1}-1-t}(\theta-\xi^T(t)\xi(t)))>0,\quad 0\le r\le s-1.\tag{23}$$

Hence, it can be derived that

$$\begin{aligned}&\alpha^{k_s-k_{r+1}+1}\sum_{t=k_r}^{k_{r+1}-1}(\alpha^{k_{r+1}-1-t}(\theta-\xi^T(t)\xi(t)))\\=&\sum_{t=k_r}^{k_{r+1}-1}(\alpha^{k_s-t}(\theta-\xi^T(t)\xi(t)))\\>&0,\end{aligned}\tag{24}$$

$$\begin{aligned}&\sum_{r=0}^{s-1}\sum_{t=k_r}^{k_{r+1}-1}(\alpha^{k_s-t}(\theta-\xi^T(t)\xi(t)))\\=&\sum_{t=0}^{k_s-1}(\alpha^{k_s-t}(\theta-\xi^T(t)\xi(t)))\\>&0,\end{aligned}\tag{25}$$

and

$$\begin{aligned}&\alpha^{k-k_s}\sum_{t=0}^{k_s-1}(\alpha^{k_s-t}(\theta-\xi^T(t)\xi(t)))\\=&\sum_{t=0}^{k_s-1}(\alpha^{k-t}(\theta-\xi^T(t)\xi(t)))\\>&0.\end{aligned}\tag{26}$$

According to (5), (6), and (26), we obtain

$$\sum_{t=0}^{k}(\alpha^{k-t}\theta)>\sum_{t=0}^{k}(\alpha^{k-t}\xi^T(t)\xi(t)),\tag{27}$$

which implies that

$$\begin{aligned}\left(\frac{\theta}{1-\alpha}\right)&>\left(\sum_{t=0}^{k}(\alpha^{k-t}\theta)\right)\\&>\left(\sum_{t=0}^{k}(\alpha^{k-t}\xi^T(t)\xi(t))\right)\\&=\left(\alpha\sum_{t=0}^{k-1}(\alpha^{k-t-1}\xi^T(t)\xi(t))+\xi^T(k)\xi(k)\right)\\&>\xi^T(k)\xi(k).\end{aligned}\tag{28}$$

Summing up both sides of (22) from $k=0$ to $k=\mathcal{T}-1$, it can be deduced that

$$\begin{aligned}&\mathbb{E}\left\{\sum_{k=0}^{\mathcal{T}-1}(\Delta V(k))\right\}=\mathbb{E}\{V(\mathcal{T})-V(0)\}\\<&\mathbb{E}\left\{\sum_{k=0}^{\mathcal{T}-1}(\mathcal{J}^T(k)\mathscr{H}(k)\mathcal{J}(k))\right\}\\<&\mathbb{E}\left\{\sum_{k=0}^{\mathcal{T}-1}\left(\mathcal{J}^T(k)\mathscr{H}(k)\mathcal{J}(k)+a_1\frac{\theta}{1-\alpha}-a_1\xi^T(k)\xi(k)\right.\right.\\&+z^T(k)z(k)-\bar{\omega}^T(k)\Gamma(k)\bar{\omega}(k)-z^T(k)z(k)\\&\left.\left.+\bar{\omega}^T(k)\Gamma(k)\bar{\omega}(k)\right)\right\}\\=&\mathbb{E}\left\{\sum_{k=0}^{\mathcal{T}-1}\left(\mathcal{J}^T(k)\Lambda(k)\mathcal{J}(k)\right)+\sum_{k=0}^{\mathcal{T}-1}\left(\bar{\omega}^T(k)\Gamma(k)\bar{\omega}(k)\right.\right.\\&\left.\left.-z^T(k)z(k)+a_1\frac{\theta}{1-\alpha}\right)\right\}.\end{aligned}\tag{29}$$

Then, we have

$$\begin{aligned}
&\mathbb{E}\Big\{\sum_{k=0}^{\mathcal{T}-1}(z^T(k)z(k))\Big\}\\
<&\mathbb{E}\{V(0)\}-\mathbb{E}\{V(\mathcal{T})\}+\mathbb{E}\Big\{\sum_{k=0}^{\mathcal{T}-1}\big(\bar{\omega}^T(k)\bar{\omega}(k)\\
&+a_1\frac{\theta}{1-\alpha}\big)\Big\}\\
<&\mathbb{E}\Big\{\zeta^T(0)P(0)\zeta(0)+\sum_{k=0}^{\mathcal{T}-1}\big(\bar{\omega}^T(k)\Gamma(k)\bar{\omega}(k)+a_1\frac{\theta}{1-\alpha}\big)\Big\}.
\end{aligned}\tag{30}$$

Furthermore, based on (18), (19), and the initial condition $P(0)\leq\gamma^2W$, we arrive at

$$\begin{aligned}
&\mathbb{E}\left\{\sum_{k=0}^{\mathcal{T}-1}(z^T(k)z(k))\right\}\\
\leq&\mathbb{E}\left\{\gamma^2\left(\sum_{k=0}^{\mathcal{T}-1}\left(\bar{\omega}^T(k)\bar{\omega}(k)+\varrho+\zeta^T(0)W\zeta(0)\right)\right)\right\}.
\end{aligned}\tag{31}$$

The proof is complete. □

Theorem 1 has provided a sufficient condition under which the closed-loop system (4) satisfies the prescribed finite-horizon H_∞ performance under the given controller gains. It is worth noting that the matrix inequalities in Theorem 1 involve nonlinear terms, making it difficult to solve. To address this issue, Theorem 2 is presented, in which the controller gain can be directly computed via the linear matrix inequality (LMI) technique.

Theorem 2. *Let positive scalars $\gamma>0$, $0<\alpha<1$, $\theta>0$, $\varrho>0$, and a positive definite matrix W be given. Assume that there exist matrices $K(k)$, $P(k)$, $\Gamma(k)$ $(k=0,1,\ldots,\mathcal{T}-1)$, and a scalar a_1 such that, under the initial conditions $P(0)\leq\gamma^2W$, the following matrix inequalities are satisfied:*

$$\begin{bmatrix}\Lambda_1(k) & \mathcal{N}^T(k)\\ * & \bar{\mathcal{P}}(k+1)\end{bmatrix}<0 \tag{32}$$

$$\Gamma(k)<\gamma^2I \tag{33}$$

$$a_1\frac{\theta}{1-\alpha}\leq\gamma^2\varrho \tag{34}$$

for each $k\in[0,\mathcal{T}-2]$, where

$$\begin{aligned}
\Lambda_1(k)&=\begin{bmatrix}-P(k)+M^T(k)M(k) & 0 & 0\\ * & -\Gamma(k) & 0\\ * & * & -a_1(k)\end{bmatrix},\\
\bar{\mathcal{P}}(k+1)&=\begin{bmatrix}P(k+1)-2I & 0\\ 0 & P(k+1)-2I\end{bmatrix},\\
\mathcal{N}(k)&\triangleq\begin{bmatrix}\mathcal{A}_1(k) & \mathcal{L}_1(k) & -\mathcal{A}_5(k)\\ \sqrt{\check{\alpha}}\mathcal{A}_2(k) & \sqrt{\check{\alpha}}\mathcal{L}_2(k)+\sqrt{\check{\tau}}\mathcal{L}_3(k) & -\sqrt{\check{\alpha}}\mathcal{A}_6(k)\end{bmatrix}.
\end{aligned}$$

Then, the system (15) meets the finite-horizon H_∞ performance (16).

Proof. $\Lambda(k)$ can be written as follows:

$$\Lambda(k)=\Lambda_1(k)+\mathcal{N}^T(k)\mathcal{P}(k+1)\mathcal{N}(k) \tag{35}$$

where

$$\mathcal{P}(k+1)=\begin{bmatrix}P(k+1) & 0\\ 0 & P(k+1)\end{bmatrix}.$$

According to the well-known Schur complement lemma, (35) can be rewritten as

$$\Lambda(k)=\begin{bmatrix}\Lambda_1(k) & \mathcal{N}^T(k)\\ \mathcal{N}(k) & -\mathcal{P}^{-1}(k+1)\end{bmatrix}<0. \tag{36}$$

Then, based on $(Z^T-S)S^{-1}(Z^T-S)^T=Z^TS^{-1}Z-Z^T-Z+S\geq 0$, (36) can be expressed as (32), which completes the proof. □

Remark 3. *Up to this point, the finite-horizon H_∞ control problem has been addressed for the mobile robot under the AETM and hybrid cyber attacks. To be specific, Theorem 1 has provided a sufficient condition under which the mobile robot achieves the prescribed control performance under the designed controller, while Theorem 2 has presented a method for computing the controller gain.*

Remark 4. *Compared with the existing studies on control problems for mobile robots, this paper presents the following notable contributions:*

(1) This is the first work to introduce the AETM into the control problem for mobile robots. Compared with traditional ETMs, AETM offers two key advantages: enhanced robustness against abrupt signal changes and a lower transmission frequency, thereby enabling more efficient scheduling of data transmission from sensors to the controller.

(2) A more general form of cyber attacks (referred to as hybrid cyber attacks) is considered. A sufficient condition is established to guarantee that the mobile robot meets the prescribed control performance under the combined influence of AETM and such attacks.

(3) A time-varying controller gain is given by recursively solving a series of matrix inequalities, which facilitates practical implementation.

4. An Illustrative Example

In this section, the kinematic model of the mobile robot is employed to validate the effectiveness of the proposed control strategy. The parameters of the robot are set as follows:

$$T=0.1\text{s},\theta_r\left(k\right)=0.005,$$
$$v_r=0.45\text{m/s},l=0.4\text{m}.$$

Then, the following settings are adopted:

$$A(k)=\begin{bmatrix}1 & 0 & -0.01\sin(0.01k)\\ 0 & 1 & 0.01\cos(0.01k)\\ 0 & 0 & 1\end{bmatrix},$$
$$B(k)=\begin{bmatrix}0.1\cos(0.01k) & 0\\ 0.1\sin(0.01k) & 0\\ \tan(0.01k) & \frac{0.01}{\cos^2(0.1k)}\end{bmatrix},$$
$$C\left(k\right)=\begin{bmatrix}0.6 & 0.03 & -0.04\\ 0.06 & 0.7 & 0.65\\ 0.1 & 0.1 & 0.8\end{bmatrix},$$
$$M\left(k\right)=\begin{bmatrix}0.04 & -0.07 & 0.05\end{bmatrix},$$
$$E\left(k\right)=\begin{bmatrix}0.08 & 0 & 0\\ 0 & 0.07 & 0\\ 0 & 0 & 0.09\end{bmatrix},D\left(k\right)=\begin{bmatrix}0.02\\ 0.24\\ 0.01\end{bmatrix}.$$

The matrix $P(0)$, the initial state $x(0)$, the initial input $u(0)$, the attack probabilities $\bar{\alpha}$ and $\bar{\beta}$, the threshold parameter θ, the weighting coefficient α, and the performance index parameter γ^2 are given as follows:

$$P\left(0\right)=\begin{bmatrix}6.8 & 0.01 & -0.01\\ 0.01 & 0.3 & 0.02\\ -0.01 & 0.02 & 1\end{bmatrix},$$
$$x\left(0\right)=\begin{bmatrix}0.2 & -0.025 & 0.135\end{bmatrix}^T,u\left(0\right)=\begin{bmatrix}0.2 & 0.3\end{bmatrix}^T,$$
$$\bar{\alpha}=0.6,\ \bar{\beta}=0.25,\ \theta=0.00031,\ \alpha=0.9,\ \gamma^2=0.5.$$

$\omega(k)$, $\nu(k)$, and $\varsigma(k)$ are set as:

$$\omega(k) = \begin{bmatrix} 0.15\sin(k) & 0.1\sin(0.8k) & 0.2\cos(k) \end{bmatrix},$$
$$\nu(k) = 0.03\sin(k), \varsigma(k) = \begin{bmatrix} 0.15\sin(k) \\ 0.1\sin(0.8k) \\ 0.2\cos(k) \end{bmatrix}.$$

The simulation runs for 100 steps, with results illustrated in the figures below. As shown in Figures 3 and 4, the position errors along the x-axis ($x_1(k)$) and y-axis ($x_2(k)$), the heading angle error ($x_3(k)$), and the control inputs $u(k)$ gradually converge to zero over time under the proposed controller.

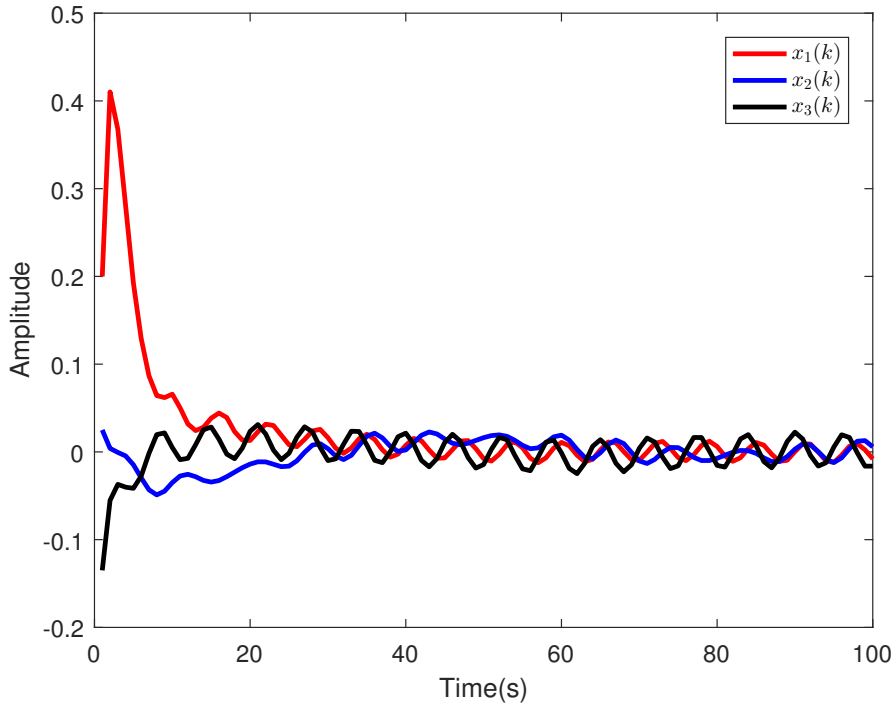

Figure 3. Trajectories of $x_1(k)$, $x_2(k)$, and $x_3(k)$.

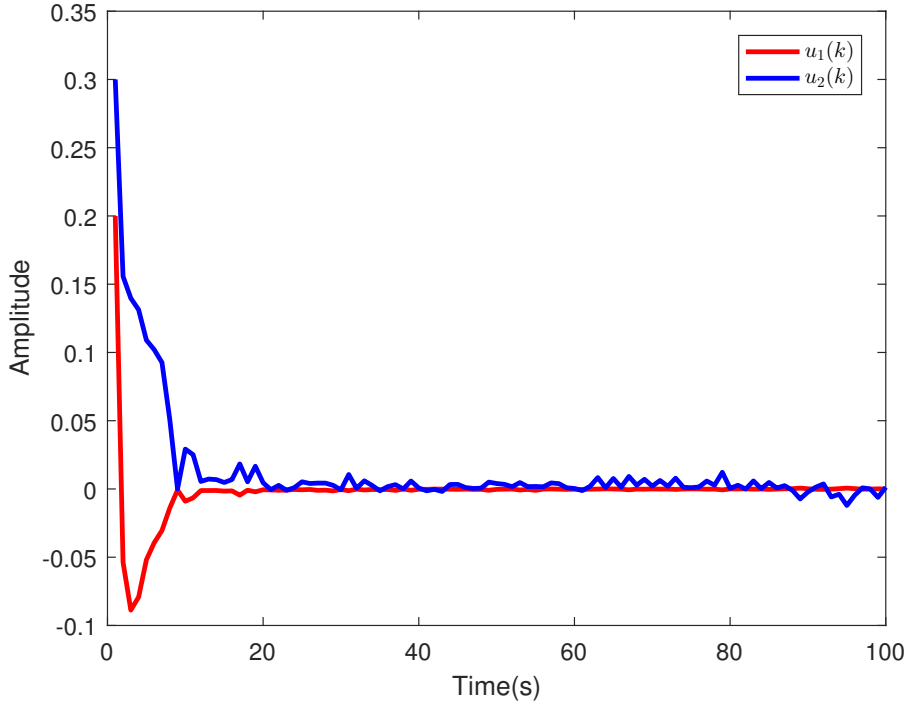

Figure 4. Control input $u(k)$.

Figure 5 demonstrates accurate trajectory tracking of the mobile robot achieved with the proposed control strategy, while Figure 6 illustrates the triggering sequences of hybrid cyber attacks (combining DoS and deception attacks). As shown in Figures 3–5, it can be clearly observed that under the proposed algorithm, the mobile robot achieves superior trajectory tracking performance even in the presence of DoS and deception attacks, which demonstrates the effectiveness of the proposed approach. Figure 7 compares triggering instants between the AETM and traditional ETM, revealing a critical finding: the AETM significantly reduces triggering frequency while maintaining identical control performance. This indicates that the proposed triggering strategy effectively alleviates communication burdens and optimizes resource utilization under adversarial conditions.

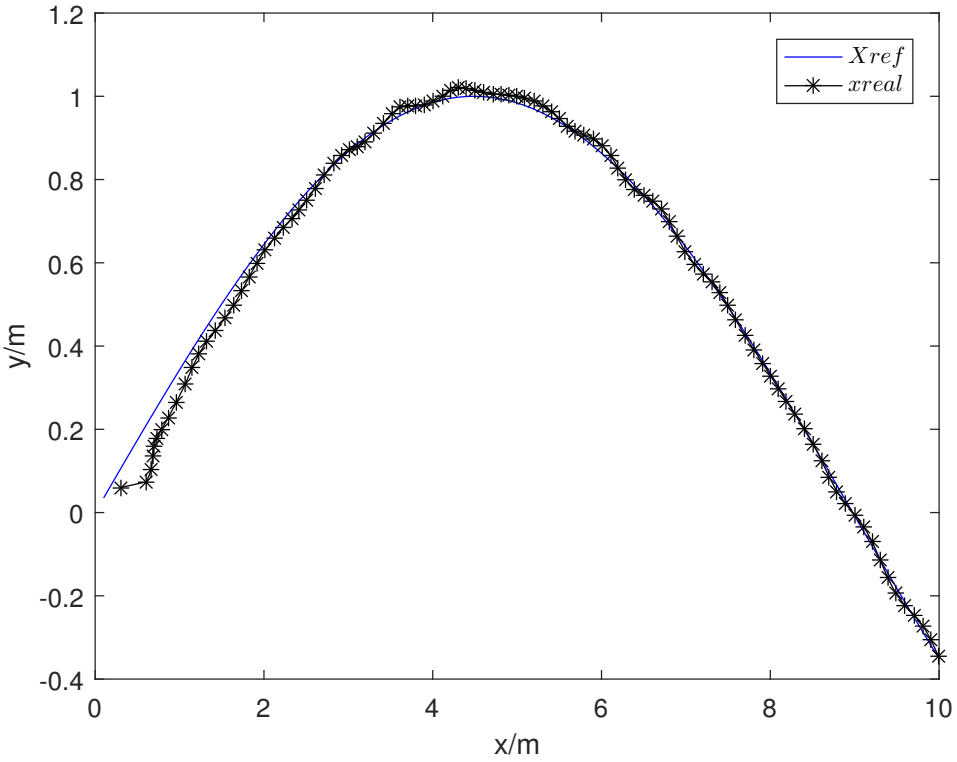

Figure 5. Trajectory tracking results of the mobile robot.

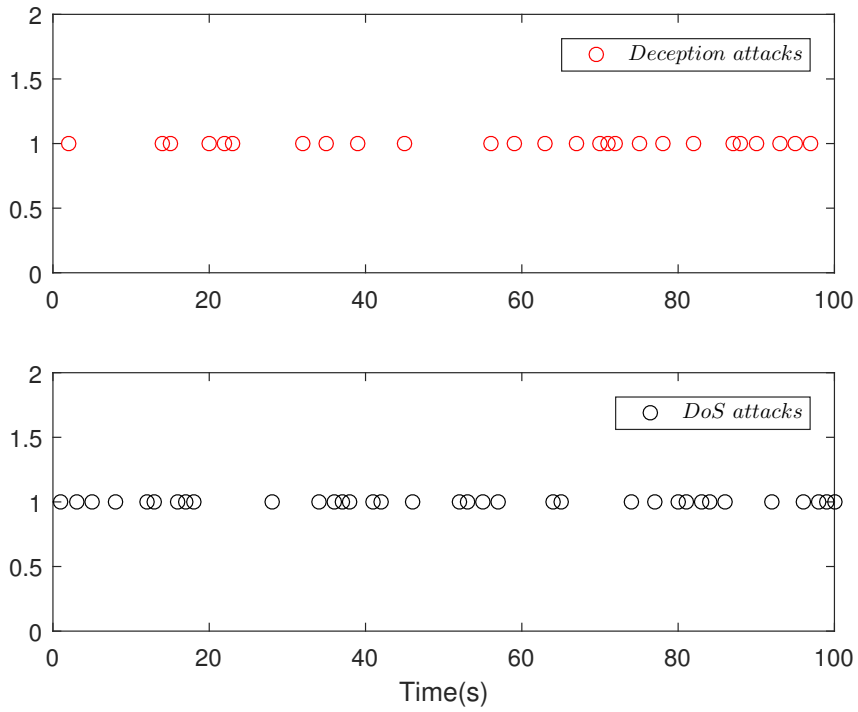

Figure 6. Time instants when the DoS attack and the deception attack occur.

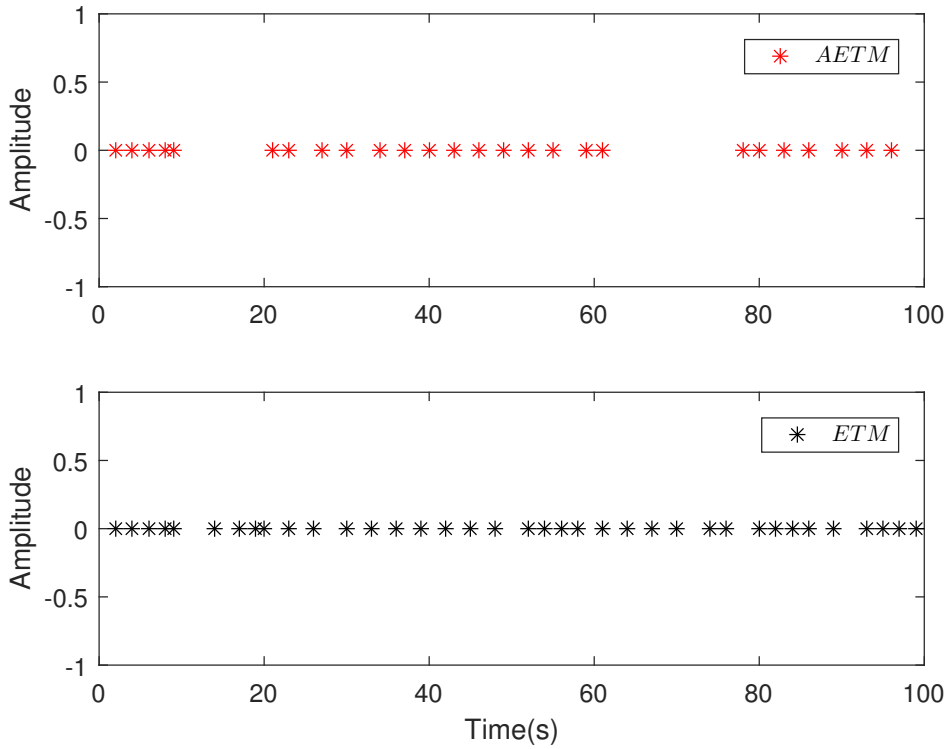

Figure 7. Triggering instants under the AETM and the traditional ETM.

To further validate efficiency improvements, 50 Monte Carlo simulations evaluate the average number of data transmissions under both AETM and traditional ETM. Table 1 summarizes the results, where N^* denotes transmission counts. As evidenced in Table 1, the AETM substantially reduces data transmission frequency compared to the traditional ETM, thereby conserving communication resources.

Table 1. Triggering times under the AETM and the traditional ETM.

Schemes	N^*
Traditional ETM	34.25
AETM	20.35

5. Conclusions

In this paper, the finite-horizon H_∞ control problem has been thoroughly addressed for mobile robots under AETMs and hybrid cyber attacks. The AETM employed in this paper is more robust to abrupt signal changes and operates at a lower transmission frequency compared to traditional ETMs. The hybrid attack model considered in this paper is more general than a single cyber attack, providing a more comprehensive representation of the complexity of network threats. Under the combined influence of the AETM and the hybrid cyber attacks, sufficient conditions have been established to ensure that the mobile robot can achieve the prescribed finite-horizon H_∞ performance under the designed controller. Based on this, the controller gain has been obtained by recursively solving a series of matrix inequalities. Finally, simulation experiments based on the kinematic model of the mobile robot have been conducted to verify the effectiveness of the proposed control strategy.

In future work, we would pay more attention to the potential research issues include addressing the trajectory tracking problem for mobile robots operating under covert attacks and AETMs [26,27], tackling control challenges for mobile robots under amplify-and-forward relays and AETMs [28,29], and the consensus control problem for multi-agent systems under AETMs [30,31].

Author Contributions: B.S. (Baoye Song): conceptualization, methodology, supervision, writing—reviewing and editing; B.S. (Bingna Sun): data curation, writing—original draft preparation, software; J.Z.: visualization, investigation.

Funding: This work was supported in part by the Natural Science Foundation of Shandong Province of China under Grant ZR2023MF067 and the National Natural Science Foundation of China under Grant 61933007.

Data Availability Statement: Not applicable.

Conflicts of Interest: The authors take full responsibility for the content of the published article.

Use of AI and AI-Assisted Technologies: No AI tools were utilized for this paper.

References

1. Yao, M.; Deng, H.; Feng, X. Improved Dynamic Windows Approach Based on Energy Consumption Management and Fuzzy Logic Control for Local Path Planning of Mobile Robots. *Comput. Ind. Eng.* **2024**, *187*, 109767.
2. Sun, Z.; Han, C. Linear State Estimation for Multi-Rate NCSs with Multi-Channel Observation Delays and Unknown Markov Packet Losses. *Int. J. Netw. Dyn. Intell.* **2025**, *4*, 100005.
3. Chen, Y.; Wang, W.; Xu, J. Robust H_∞ Estimation for 2D FMLSS Systems under Asynchronous Multi-Channel Delays: A Partition Reconstruction Approach. *Int. J. Netw. Dyn. Intell.* **2024**, *4*, 100017.
4. Yang, Y.; Niu, Y.; Li, J. Fuzzy Modeling and Event-Triggered Control of Offshore Platforms under Constrained Bandwidth: An Encoding-Decoding Scheme. *Nonlinear Dyn.* **2025**, *113*, 21359–21382.
5. Mohammadzadeh, A.; Tavassoli, B. Optimal Linear Filter Design for Process State and Packet Loss Estimation in Networked Control Systems. *ISA Trans.* **2024**, *147*, 79–89.
6. Wen, B.; Huang, J. Event-Trigger-Based Composite Leader-Following Consensus Control for Stochastic Multi-Agent Systems. *Eur. J. Control* **2025**, *84*, 101251.
7. Bai, X.; Li, G.; Ding, M.; et al. Recursive Strong Tracking Filtering for Power Harmonic Detection with Outliers-Resistant Event-Triggered Mechanism. *Int. J. Netw. Dyn. Intell.* **2024**, *3*, 100023.
8. Wang, W.; Wang, M. Adaptive Neural Event-Triggered Output-Feedback Optimal Tracking Control for Discrete-Time Pure-Feedback Nonlinear Systems. *Int. J. Netw. Dyn. Intell.* **2024**, *3*, 100010.
9. Ren, J.; Hua, L.; Zhao, M. Bipartite Consensus for Multi-Agent Systems Over Signed Networks: A Novel Dynamic Event-Triggered Mechanism. *Neurocomputing* **2024**, *609*, 128502.
10. Åström, K.J.; Bernhardsson, B. Comparison of Periodic and Event-Based Sampling for First-Order Stochastic Systems. *IFAC Proc. Vol.* **1999**, *32*, 5006–5011.
11. Zhang, L.; Nguang, S.K.; Quyang, D. Synchronization of Delayed Neural Networks via Integral-Based Event-Triggered Scheme. *IEEE Trans. Neural Netw. Learn. Syst.* **2020**, *31*, 5092–5102.
12. Girard, A. Dynamic Triggering Mechanisms for Event-Triggered Control. *IEEE Trans. Autom. Control* **2015**, *60*, 1992–1997.
13. Shi, Y.; Tian, E.; Shen, S. Adaptive Memory-Event-Triggered Control for Network-Based T-S Fuzzy Systems with Asynchronous Premise Constraints. *IET Control Theory Appl.* **2021**, *15*, 534–544.
14. Guo, J.; Liu, H.; Hu, J.; et al. Joint State and Actuator Fault Estimation for Networked Systems under Improved Accumulation-Based Event-Triggered Mechanism. *ISA Trans.* **2022**, *127*, 60–67.
15. Liu, F.; Wang, C.; Geng, Q. Observer-Based MPC for NCS with Actuator Saturation and DoS Attacks via Interval Type-2 T-S Fuzzy Model. *IET Control Theory Appl.* **2020**, *14*, 3537–3546.
16. Zhang, H.; Pan, S.; Li, T. Switching-Like Event-Triggered Tracking Control for UAH/UGV Systems under External Disturbance and DoS Attacks. *Int. J. Robust Nonlinear Control* **2024**, *34*, 6259–6283.
17. Li, J.; Mu, X.; Li, K. Event-Triggered Finite-Time Bounded and Finite-Time Stability for Networked Control Systems under DoS Attacks. *Int. J. Syst. Sci.* **2020**, *51*, 2820–2836.
18. Gamage, D.; Wanigasekara, C.; Ukil, A. Distributed Consensus Controlled Multi-Battery-Energy-Storage-System under Denial-of-Service Attacks. *J. Energy Storage* **2024**, *86*, 111180.
19. Wu, Z.; Xiong, J.; Xie, M. Dynamic Event-Triggered L_∞ Control for Networked Control Systems under Deception Attacks: A Switching Method. *Inf. Sci.* **2021**, *561*, 168–180.
20. Mizinov, P.V.; Konnova, N.S.; Basarab, M.A. Parametric Study of Hand Dorsal Vein Biometric Recognition Vulnerability to Spoofing Attacks. *J. Comput. Virol. Hacking Tech.* **2024**, *20*, 383–396.
21. Yu, Y.; Yang, W.; Ding, W. Reinforcement Learning Solution for Cyber-Physical Systems Security Against Replay Attacks. *IEEE Trans. Inf. Forensics Secur.* **2023**, *18*, 2583–2595.
22. Veesa, S.; Singh, M. Implicit Processing of Linear Prediction Residual for Replay Attack Detection. *Int. J. Speech Technol.* **2024**, *27*, 781–791.
23. Mokari, H.; Firouzmand, E.; Sharifi, I. Resilient Control Strategy and Attack Detection on Platooning of Smart Vehicles under DoS Attack. *ISA Trans.* **2024**, *144*, 51–60.
24. Han, X.; Xiong, J.; Shen, W. The Perils of Wi-Fi Spoofing Attack via Geolocation API and Its Defense. *IEEE Trans. Dependable Secure Comput.* **2024**, *21*, 4343–4359.
25. Jia, X.; Li, H.; Chi, X. Edge-Based Dynamic Event-Triggered Leader-Following Output Consensus of Uncertain Heterogeneous Multi-Agent Systems with Multi-Channel Hybrid Cyber-Attacks. *IEEE Trans. Syst. Man Cybern. Syst.* **2024**, *54*, 5543–5555.
26. Wu, Z.; Tian, E.; Chen, H. Covert Attack Detection for LFC Systems of Electric Vehicles: A Dual Time-Varying Coding Method. *IEEE/ASME Trans. Mechatron.* **2023**, *28*, 681–691.
27. Li, X.; Zhang, P.; Dong, H. A Robust Covert Attack Strategy for a Class of Uncertain Cyber-Physical Systems. *IEEE Trans. Autom. Control* **2024**, *69*, 1983–1990.

28. Jia, C.; Hu, J.; Yi, X.; et al. Recursive State Estimation for a Class of Quantized Coupled Complex Networks Subject to Missing Measurements and Amplify-and-Forward Relay. *Inf. Sci.* **2023**, *630*, 53–73.
29. Hu, J.; Li, J.; Yan, H.; et al. Optimized Distributed Filtering for Saturated Systems with Amplify-and-Forward Relays over Sensor Networks: A Dynamic Event-Triggered Approach. *IEEE Trans. Neural Netw. Learn. Syst.* **2023**, *35*, 17742–17753.
30. Zhong, Y.; Zhang, Y.; Ge, S.S.; et al. Robust Distributed Sensor Fault Detection and Diagnosis within Formation Control of Multiagent Systems. *IEEE Trans. Aerosp. Electron. Syst.* **2023**, *59*, 1340–1353.
31. Wang, Y.; Lu, J.; Liang, J. Security Control of Multiagent Systems under Denial-of-Service Attacks. *IEEE Trans. Cybern.* **2022**, *52*, 4323–4333.